Supporting Information

Modulating LOV domain photodynamics with a residue alteration outside the chromophore binding site

Sang-Hun Song, Peter L. Freddolino, Abigail I. Nash, Elizabeth C. Carroll, Klaus Schulten, Kevin H. Gardner, Delmar S. Larsen

SI1: Cloning, Expression, and Purification of AsLOV2

DNA encoding *Avena sativa* phototropin 1 LOV2 domain plus the C-terminal Jα helix (residues 404-560)[1] was used to generate the F434Y mutant. Mutagenesis was carried out according to the Quick Change II XL site-directed mutagenesis kit (Stratagene) following manufacturer's instructions and verified by DNA sequencing. Proteins were expressed in *E. coli* BL21(DE3) cells grown in LB broth at 37°C to an A_{600} of 0.6-0.8 and then induced with IPTG (0.12 g/L). After 16 hr induction at 20°C, cells were centrifuged and pellets resuspended in 50 mM Tris (pH 8.0), 100 mM NaCl buffer. Cells were lysed using sonication and clarified with centrifugation at 48,000 g for 30 min. The soluble fraction was loaded onto a High Performance Ni^{2+}-Sepharose (Amersham) column, allowing for rapid affinity purification of His-Gβ1 tagged (*1*) AsLOV2 fusions by eluting with 250 mM imidazole. After exchanging the LOV-containing fractions into 50 mM Tris (pH 8.0), 100 mM NaCl buffer, the His-Gβ1 tag was cleaved by adding 1 mg His_6-TEV protease per 30 mg of fusion protein. Proteolysis reactions were allowed to proceed overnight at 4°C and stopped using a High Performance Ni^{+2}-Sepharose column to remove the His-Gβ1 and His_6-TEV protease. Protein was then concentrated and injected onto a Superdex 75 column for final purification and exchange into 50 mM sodium phosphate (pH 6.0),

100 mM NaCl buffer. The resulting purified proteins contain only the GEF (N-terminal) and G (C-terminal) residues as cloning artifacts. Although the photodynamics of oxidized flavin in aqueous solution are strongly affected by dissolved oxygen (*2*), the protein binding pocket of FMN sufficiently excludes oxygen to not appreciably affect measured photodynamics (*3*) and no efforts to deoxygenate the samples were made.

SI2: Molecular dynamics simulations

Initial structures for the residue 403-536 fragment of *A. sativa* LOV2 were generated based on the room temperature crystal structures of Halavaty and Moffat (PDB codes 2V1A and 2V1B for the dark and light states, respectively) (*4*). In both cases the crystal structures of the protein and chromophore were used and all water and other cofactors discarded. An initial solvation shell was added using SOLVATE 1.2 (*5*) with padding extending 15 Å beyond the protein; a solvent cube was completed using the solvate module of VMD 1.8.6 (*6*), and a minimal set of neutralizing ions (6 sodium ions) placed using the autoionize plugin of VMD 1.8.6. After ionization, the appropriate F434Y structures were generated by point mutation of residue 434; the structures used are identical to those of the wildtype simulations (*7*).

Molecular dynamics (MD) simulations were performed using an alpha version of NAMD 2.7 (*8*) . In all cases the CHARMM22 force field with CMAP corrections was used for the protein and ions (*9, 10*), water treated using the TIP3P water model (*11*), and newly derived flavin and cysteinyl-flavin photoadduct parameters (*7*) used for the chromophore. All hydrogen-containing bonds in the protein and chromophore were constrained in length using RATTLE (*12*) and rigid water geometries maintained with SETTLE (*13*). Short-range nonbonded interactions were cut

off at 10.0 Å with switching starting at 9.0 Å; long-range electrostatics were treated using the Particle Mesh Ewald method with a grid spacing no greater than 1.0 $Å^{-1}$ along each axis. A timestep of 2.0 fs was used in all cases to integrate the equations of motion, and multiple timestepping employed to evaluate long range electrostatics once every two steps. All simulations were performed in the isothermal-isobaric ensemble; a constant temperature of 298 K was maintained using a Langevin thermostat with a damping constant of 5.0 ps^{-1} during equilibration and 1.0 ps^{-1} during production runs, and a pressure of 1.0 atm enforced using a Nosé-Hoover Langevin piston barostat (*8*) with a period of 200 fs and decay time of 100 fs. Coordinates were saved to disk once every two ps during the trajectory.

Prior to production runs, the dark and light state F434Y systems were equilibrated in a two stage process: All protein and chromophore atoms were first restrained to their crystal coordinates with a spring constant of 10.0 kcal/(mol $Å^2$), and the backbone atoms of the protein constrained to their initial coordinates. The system was minimized for 3000 steps, equilibrated for 200 ps, and the restraints on the protein non-backbone atoms were removed in ten steps over an additional 200 ps of simulation. The backbone constraints were then changed to harmonic restraints, and removed in ten successive steps over another 200 ps of simulation. Equilibration was completed on the fully unrestrained system with an additional 100 ps of dynamics propagation.

For both the dark and light state LOV2-F434Y systems, three independent 200 ns simulations were performed using identical coordinates but different initial velocities and sets of random seeds. These trajectories are referred to as D_F434Y1, D_F434Y2, D_F434Y3, L_F434Y1, L_F434Y2, and L_F434Y3 for the dark (D_) and light state (L_) trajectories. The five dark and light state wildtype AsLOV2 trajectories simulated independently (*7*), obtained under near-

identical conditions to the simulations presented here, are referred to as D_WT1-5 and L_WT1-5.

Oxygen accessibilities were calculated using the implicit ligand sampling (ILS) method of Cohen and co-workers (*15*). ILS was performed on the concatenation of all trajectories for each of the D_WT, L_WT, D_F434Y, and L_F434Y, excluding the first 20 ns of each trajectory. Free energies were obtained on a lattice with a spacing of 0.1 nm on each dimension, with 27x supersampling (3x along each dimension) and a set of 20 orientations used at each of the (super-sampled) grid points. The trajectories were aligned by the LOV domain core (residues 416-516) prior to ILS calculations.

The difference in the stability of the photoadduct in the wildtype and F434Y cases was determined by taking the difference of the ΔG values for mutating F434 to tyrosine in the light and dark states with the free energy perturbation (FEP) module of NAMD 2.7; in such calculations a scaling parameter is used to transition between the initial (λ=0) and final (λ=1) states. Intermediates were taken at λ = 0.0, 0.1, 0.2... 0.9, 1.0, and one additional intermediate at λ = 0.85 was used in the dark state to improve overlaps of adjacent ensembles. For each transition between adjacent intermediates, 1 ns of sampling was performed after 100 ps of equilibration. A soft core potential was used for van der Waals interactions (*14*). Free energy differences were then calculated using the bidirectional Bennett acceptance ratio (BAR) (*16*). In the case of the dark state FEP, in order to accelerate convergence all sampling was performed with an added CHARMM-style dihedral term restraining the χ_1 angle of residue Cys450 to the mode value for the conformation I rotamer with a force constant of 10 kcal/mol. The effects of this restraint were removed at the endpoints using a BAR calculation with data only from the

unrestrained ensembles (*i.e.*, the 1000 ns and 600 ns equilibrium trajectories of the WT and F434Y systems, respectively).

SI3: Gln 513 Dynamics

The major conformational states (and their populations) of Gln513 encountered in wildtype AsLOV2 and F434Y from the MD simulation are shown in Fig. SI1. Notably, as expected based on the introduction of an extra hydrogen bond acceptor above the plane of FMN, Gln513 takes on a light-like conformation even in the F434Y dark state, showing rotation away from FMN due to the presence of a bound water (Fig. SI1, conformation v); the population from the dark-adapted F434Y system showing similar distance/dihedral combinations to conformation iii in Fig. SI1 is actually more similar to conformation iv, but with a different Gln513 rotamer. The conformation of Gln513 in the F434Y light state is not strongly affected, although it does show a form of conformation iv which is even more distant from FMN than in the wildtype. As was observed in the light-induced wildtype simulations, conformations of Gln513 which are turned away from FMN in the F434Y dark state are correlated with tilting of the Iβ strand and an increased population of states where the C-terminal portion of the Jα helix separates from the LOV domain core (data not shown). However, other light-induced structural changes observed in Reference 7 to be linked to the early stages of Jα dissociation were not observed. It is thus unclear, in the absence of experimental data or simulated Jα dissociation, what effect the F434Y mutation has on the stability of the AsLOV2-Jα interface.

The correlations between water binding site occupancies and the conformation of Q513 are shown in Table SI1, using the Q513-O4 hydrogen bonding distance to track the orientation of the Q513 side chain. For the purposes of that table, a water is defined as being in the O4 binding site

if its oxygen is within 3.5 Å of the FMN O4 atom, in the N5 binding site if its oxygen is within 3.5 Å of the FMN N5 atom, and in the antechamber site if its oxygen is simultaneously within 5 Å of N414 and N492. Statistics are calculated for a concatenation of the last 120 ns of each trajectory falling into a given category (*e.g.*, the statistics for the dark state F434Y simulations combine the last 120 ns of each of trajectories D_F434Y1-3). Error bars are given as two times the standard error of the mean, treating each nonoverlapping 10 ns slice of trajectory as a single independent data point.

SI4: Solution NMR spectroscopy

Solution NMR utilized uniformly ^{15}N-labeled protein, generated from bacteria grown in M9 minimal media containing 1 g/L of $^{15}NH_4Cl$. Solution NMR experiments were performed on Varian Inova 600 and 800 MHz spectrometers at 25°C, using nmrPipe[17] for data processing and NMRview[18] for analysis. Sensitivity-enhanced ^{15}N/^{1}H HSQC spectra[19] were acquired on samples between 200-500 micromolar concentration, with total experimental time being approximately 30-60 minutes apiece.

SI5: Chemical Shift Difference Map

To evaluate the structural effects of the F434Y point mutation, we analyzed ^{15}N/^{1}H HSQC solution NMR spectra collected on uniformly ^{15}N-labeled samples of F434Y AsLOV2 and compared these to corresponding spectra of wildtype AsLOV2 (*1*). Qualitative comparisons of these spectra (Fig. SI2a) reveal minimal changes, with a similar overall pattern of crosspeaks from ^{15}N/^{1}H pairs (chiefly backbone and sidechain amides, and tryptophan indoles) distributed throughout the protein. To obtain a more quantitative examination of perturbations, we performed minimum chemical shift analysis (*17*) to establish the minimal degree of perturbation

of the chemical shift assignments of the wildtype AsLOV2[1] necessary to obtain the F434Y spectra. Chemical shift perturbations were established by weighing the change in chemical shift (in ppm) as follows:

$$\Delta\delta_{mcs} = \mathrm{sqrt}((\Delta\delta_{min}(^{1}H))^2 + (0.1*\Delta\delta_{min}(^{15}N))^2)$$

where $\Delta\delta_{min}$ is the minimal chemical shift required in each dimension associated with moving from an assigned crosspeak (in AsLOV2) to the nearest peak in F434Y spectra. Results from this analysis, which provides a conservative estimate of chemical shift changes, indicate a heterogeneous response to the point mutation (Fig. SI2b).

Mapping the minimum chemical shift results on the crystal structure of dark state AsLOV2 (Fig. SI2c)[4] indicates that several of the sites that are strongly perturbed ($\Delta\delta_{mcs}$>0.2 ppm) are located in the immediate vicinity of F434 (*e.g.* A430, S431, T438, I445, L453). Notably, several sites at longer distances are also perturbed (*e.g.* I532, located approximately 13 Å from the site of mutation), suggesting that there are some minor structural changes within the protein as a whole. However, the degree of change observed in these solution NMR spectra are much less than those seen with mutations which induce dissociation of the Ja helix from the LOV domain (*1, 18*) or other major changes, suggesting that any long range changes are more subtle.

SI6: Time-Resolved Spectroscopy

The ultrafast transient absorption signals were measured with an amplified Ti:sapphire laser system (Spectra Physics Spitfire Pro and Tsunami) that delivered 800 nm pulses with an energy of 2.25 mJ at a repetition rate of 1 kHz, and 40 fs full width at half maximum (FWHM) duration. (*19*). The laser beam is split into two separate pathways for pumping and probing. The 80 nJ,

400 nm excitation pulses were generated via second harmonic generation in a β-barium borate crystal (0.1 mm thick, 29.2°). Broadband white light probe pulses were generated by focusing 800 nm pulses into a slowly translating CaF_2 crystal. The pump and probe beams were set at magic angle. The time resolution is ~100 fs (FWHM) and the spectral resolution is 1.2 nm. Both wildtype AsLOV2 and F434Y samples were suspended at concentrations of 450 μM in a buffer consisting of 50 mM sodium phosphate (pH 6.0) and 100 mM NaCl. The sample was studied in a 1 mm quartz flow cell circulated by a peristaltic pump (Watson-Marlow 406D) to refresh the sample between laser pulses. Measurements were also performed with ~3 mL of sample to avoid protein degradation and reduce the potential of re-exciting protein in the adduct state. Since the recovery of the dark state in wildtype AsLOV2 domain approximately 70 s (*20*), imidazole (200 mM) was added to induce faster recovery kinetics as demonstrated by Kennis and co-workers (*21*). However, imidazole was not used with the F434Y sample, since the recovery time scale (*vide infra*) is sufficiently rapid to ensure the probing of the dark-adapted population with each laser pulse via the sample circulation. The photodynamics for the wildtype and F434Y mutant were measured back-to-back under identical conditions including temperature and buffer composition to ensure that the resolved differences were associated exclusively with the F434Y mutation.

In the nanosecond-microsecond laser flash photolysis measurements, the samples were excited in the same 1 mm flow cell and 400 nm excitation pulses used in the fs-ns transient apparatus described above, although with a slightly higher (160 nJ) pulse energy. The ensuing photodynamics was probed with a continuous wave 640 nm laser diode (HLM1230 Class III). Transmitted probe light was detected with a 1 ns response photodiode (Thorlabs DET10A) via a

1 GHz digital oscilloscope (Tektronix TDS784A), and then transferred to a computer via National Instruments LabView software.

SI7: Simple Global fits to 10-ns Transient Data

The ultrafast signals for wildtype AsLOV2 and the F434Y mutant can be fit to simple sequential population schemes with no interconverting population flow due to isomerization of the C450 residue. The parameters of these models were used as the initial guesses for the more complex model described in the manuscript. These models do not explicitly separate internal conversion dynamics from radiative decay dynamics and intersystem crossing dynamics (Figs. SI2-5 and Table SI3). A single population model was used by Kennis and co-workers for wildtype AsLOV2, although since they were unable to resolve the FMN bleach, separation of radiative and ISC kinetics was performed after the global analysis of the data and was not experimentally resolved (*21*). The results of this simple model with single population (homogeneous) kinetics were used for the measured transient data for wildtype AsLOV2 in Figure SI4A.

As discussed in the manuscript, this same model cannot describe the F434Y sample due to the intrinsic bi-exponential nature of the signals (Fig. SI4B). Hence, a two-population model is required (Figure SI4C) to accurately describe the decay kinetics, but without incorporating the inter-conformational dynamics resolved in MD simulations, a full explanation of the extracted parameters of the model is difficult.

The Species Associated Difference Spectra (SADS) for the three models described above are contrasted in Figure SI5. For the two-population model, the SADS for each conformer were locked together to simplify the fitting. Although not necessary, this is a reasonable assumption as it is unclear how the molecular structure of each conformer would affect the resulting SADS

properties. However, it is clear from contrasting the triplet SADS for each sample that the fine details of the spectra are different between the two samples; this is ascribed to different hydrogen bonding networks between the two samples.

SI8: Adduct Recovery Signals

Purified protein was concentrated to an A_{450} of 0.3-0.4 in a 1 mm pathlength flowcell. Proteins were illuminated with multiple flashes of white light from a photographic flash followed immediately by monitoring the recovery of absorbance at 450 nm using a Varian Cary Series 50 spectrophotometer. The collected data points were fitted using a first-order rate equation to obtain the dark state recovery time constant. The photoadduct for the F434Y mutant reverts to the initial dark form (Figure SI7) with 10-fold faster time constant than wildtype (not shown).

The O_2 dependent dark recovery kinetics of F434Y AsLOV2 was measured in a Varian Cary 50 spectrophotometer equipped with an external 75 W xenon lamp source directed down over the cuvette. A photo-equilibrium of light and dark adapted states was established within 1 minute of illumination with light centered at 450 nm (70 nm FWHM). The recovery was then measured under dark conditions with the 80 Hz spectrophotometer source centered at 450 nm and a dwell time of 0.1 seconds. To test oxygen sensitivity of the dark recovery kinetics, oxygen was displaced by stirring each sample under a vented argon environment for 30 minutes. The samples were maintained under a positive pressure of Ar until immediately before the kinetics measurement, at which time the septum was removed to photoconvert the sample. A slower dark recovery was initially observed in F434Y. After 5 minutes of exposure to atmosphere, the dark recovery of the F434Y sample returned to approximately the same rate as the control sample, suggesting that the solution has become near fully saturated with O_2.

References

1. Harper, S. M., Neil, L. C., and Gardner, K. H. (2003) Structural basis of a phototropin light switch, *Science 301*, 1541-1544.
2. Song, S. H., Dick, B., and Penzkofer, A. (2007) Photo-induced reduction of flavin mononucleotide in aqueous solutions, *Chemical Physics 332*, 55-65.
3. Noll, G., Hauska, G., Hegemann, P., Lanzl, K., Noll, T., von Sanden-Flohe, M., and Dick, B. (2007) Redox properties of LOV domains: chemical versus photochemical reduction, and influence on the photocycle, *Chembiochem 8*, 2256-2264.
4. Halavaty, A. S., and Moffat, K. (2007) N- and C-terminal flanking regions modulate light-induced signal transduction in the LOV2 domain of the blue light sensor phototropin 1 from Avena sativa, *Biochemistry 46*, 14001-14009.
5. Grubmuller, H. (1996) SOLVATE 1.0 Manual.
6. Humphrey, W., Dalke, A., and Schulten, K. (1996) VMD: visual molecular dynamics, *J Mol Graph 14*, 33-38, 27-38.
7. Freddolino, P. L., Nash, A. I., Harper, S. M., Gardner, K. H., and Schulten, K. Photoreaction-induced conformational changes in A. sativa Phot1-LOV2: A molecular dynamics study, *manuscript in preparation*.
8. Phillips, J. C., Braun, R., Wang, W., Gumbart, J., Tajkhorshid, E., Villa, E., Chipot, C., Skeel, R. D., Kale, L., and Schulten, K. (2005) Scalable molecular dynamics with NAMD, *J Comput Chem 26*, 1781-1802.
9. Mackerell, A. D., Bashford, D., Bellott, M., Dunbrack, R. L., Field, M. J., Fischer, S., Gao, J., Guo, H., Ha, S., Joseph, D., Kuchnir, L., Kuczera, K., Lau, F. T. K., Mattos, C., Michnick, S., Nguyen, D. T., Ngo, T., Prodhom, B., Roux, B., Schlenkrich, M., Smith, J., Stote, R., Straub, J., Wiorkiewiczkuczera, J., and Karplus, M. (1992) Self-Consistent Parameterization of

Biomolecules for Molecular Modeling and Condensed Phase Simulations, *Faseb Journal 6*, A143-A143.

10. MacKerell, A. D., Bashford, D., Bellott, M., Dunbrack, R. L., Evanseck, J. D., Field, M. J., Fischer, S., Gao, J., Guo, H., Ha, S., Joseph-McCarthy, D., Kuchnir, L., Kuczera, K., Lau, F. T. K., Mattos, C., Michnick, S., Ngo, T., Nguyen, D. T., Prodhom, B., Reiher, W. E., Roux, B., Schlenkrich, M., Smith, J. C., Stote, R., Straub, J., Watanabe, M., Wiorkiewicz-Kuczera, J., Yin, D., and Karplus, M. (1998) All-atom empirical potential for molecular modeling and dynamics studies of proteins, *Journal of Physical Chemistry B 102*, 3586-3616.
11. Jorgensen, W. L., Chandrasekhar, J., Madura, J. D., Impey, R. W., and Klein, M. L. (1983) Comparison of Simple Potential Functions for Simulating Liquid Water, *Journal of Chemical Physics 79*, 926-935.
12. Andersen, H. C. (1983) Rattle - a Velocity Version of the Shake Algorithm for Molecular-Dynamics Calculations, *Journal of Computational Physics 52*, 24-34.
13. Miyamoto, S., and Kollman, P. A. (1992) Settle - an Analytical Version of the Shake and Rattle Algorithm for Rigid Water Models, *Journal of Computational Chemistry 13*, 952-962.
14. Zacharias, M., Straatsma, T. P., and Mccammon, J. A. (1994) Separation-Shifted Scaling, a New Scaling Method for Lennard-Jones Interactions in Thermodynamic Integration, *Journal of Chemical Physics 100*, 9025-9031.
15. Cohen, J., Arkhipov, A., Braun, R., and Schulten, K. (2006) Imaging the migration pathways for O-2, CO, NO, and Xe inside myoglobin, *Biophysical Journal 91*, 1844-1857.
16. Bennett, C. H. (1976) Efficient Estimation of Free-Energy Differences from Monte-Carlo Data, *Journal of Computational Physics 22*, 245-268.
17. Farmer, B. T., Constantine, K. L., Goldfarb, V., Friedrichs, M. S., Wittekind, M., Yanchunas, J., Robertson, J. G., and Mueller, L. (1996) Localizing the NADP+ binding site on the MurB enzyme by NMR, *Nat. Struct. Biol. 3*, 995-997.

18. Harper, S. M., Christie, J. M., and Gardner, K. H. (2004) Disruption of the LOV-Jalpha helix interaction activates phototropin kinase activity, *Biochemistry 43*, 16184-16192.

19. Carroll, E. C., Compton, O. C., Madsen, D., Osterloh, F. E., and Larsen, D. S. (2008) Ultrafast carrier dynamics in exfoliated and functionalized calcium niobate nanosheets in water and methanol, *Journal of Physical Chemistry C 112*, 2394-2403.

20. Christie, J. M., Corchnoy, S. B., Swartz, T. E., Hokenson, M., Han, I. S., Briggs, W. R., and Bogomolni, R. A. (2007) Steric interactions stabilize the signaling state of the LOV2 domain of phototropin 1, *Biochemistry 46*, 9310-9319.

21. Alexandre, M. T., Arents, J. C., van Grondelle, R., Hellingwerf, K. J., and Kennis, J. T. (2007) A base-catalyzed mechanism for dark state recovery in the Avena sativa phototropin-1 LOV2 domain, *Biochemistry 46*, 3129-3137.

22. Kottke, T., Heberle, J., Hehn, D., Dick, B., and Hegemann, P. (2003) Phot-LOV1: photocycle of a blue-light receptor domain from the green alga Chlamydomonas reinhardtii, *Biophys J 84*, 1192-1201.

23. Holzer, W., Penzkofer, A., Fuhrmann, M., and Hegemann, P. (2002) Spectroscopic characterization of flavin mononucleotide bound to the LOV1 domain of Phot1 from Chlamydomonas reinhardtii, *Photochem Photobiol 75*, 479-487.

24. Guo, H., Kottke, T., Hegemann, P., and Dick, B. (2005) The phot LOV2 domain and its interaction with LOV1, *Biophys J 89*, 402-412.

25. Kennis, J. T., Crosson, S., Gauden, M., van Stokkum, I. H., Moffat, K., and van Grondelle, R. (2003) Primary reactions of the LOV2 domain of phototropin, a plant blue-light photoreceptor, *Biochemistry 42*, 3385-3392.

26. Song, S.-H., Pullman, R., Freer, L., Brody, M., Price, C. W., and Larsen, D. S. Reformation of Photoadduct by Photoreversible Photodynamics in The YtvA-LOV Domain, *manuscript in preparation*.

27. Losi, A., Polverini, E., Quest, B., and Gartner, W. (2002) First evidence for phototropin-related blue-light receptors in prokaryotes, *Biophys J 82*, 2627-2634.

28. Islam, S. D. M., Penzkofer, A., and Hegemann, P. (2003) Quantum yield of triplet formation of riboflavin in aqueous solution and of flavin mononucleotide bound to the LOV1 domain of Phot1 from Chlamydomonas reinhardtii (vol 291, pg 97, 2003), *Chemical Physics 293*, 397-397.

Table SI1: Correlations between Q513 conformation and water occupancy in the FMN binding site from molecular dynamics simulations for wildtype AsLOV2. Each entry in the tables corresponds to the fraction of timesteps from a given simulation satisfying the corresponding properties. Water occupancies for three sites are noted: those immediately adjacent to N5, adjacent to O4 (near the crystallographic dark state side chain of Q513), and those in the antechamber site (see text for details). In all cases the Q513-FMN O4 hydrogen bond distance is used as a proxy for Q513 conformation.

Dark state, wild type (5 trajectories)									
Q513-O4 distance (Å)	O4 site occupancy (# of waters)			N5 site occupancy (# of waters)			Antechamber site occupancy (# of waters)		
	0	1	2+	0	1	2+	0	1	2+
< 3.5	0.66 ± 0.03	0.02 ± 0.01	0.00	0.68 ± 0.03	0.00	0.00	0.09 ± 0.02	0.42 ± 0.03	0.17 ± 0.02
3.5-6.5	0.16 ± 0.01	0.11 ± 0.02	0.00	0.24 ± 0.02	0.02 ± 0.01	0.00	0.08 ± 0.01	0.11 ± 0.01	0.08 ± 0.01
> 6.5	0.03 ± 0.01	0.02 ± 0.01	0.00	0.05 ± 0.01	0.00	0.00	0.04 ± 0.01	0.01 ± 0.00	0.01 ± 0.00
Light state, wild type (5 trajectories)									
Q513-O4 distance (Å)	O4 site occupancy (# of waters)			N5 site occupancy (# of waters)			Antechamber site occupancy (# of waters)		
	0	1	2+	0	1	2+	0	1	2+
< 3.5	0.23 ± 0.03	0.03 ± 0.01	0.00	0.24 ± 0.03	0.02 ± 0.01	0.00	0.02 ± 0.01	0.17 ± 0.03	0.06 ± 0.01
3.5-6.5	0.32 ± 0.03	0.30 ± 0.03	0.06 ± 0.02	0.45 ± 0.03	0.23 ± 0.03	0.00	0.29 ± 0.03	0.27 ± 0.02	0.12 ± 0.02
> 6.5	0.06 ± 0.01	0.01 ± 0.00	0.00	0.07 ± 0.01	0.00	0.00	0.05 ± 0.01	0.02 ± 0.00	0.00

Table SI2: Correlations between Q513 conformation and water occupancy in the FMN binding site from molecular dynamics simulations for F434Y AsLOV2. Each entry in the tables corresponds to the fraction of timesteps from a given simulation satisfying the corresponding properties. Water occupancies for three sites are noted: those immediately adjacent to N5, adjacent to O4 (near the crystallographic dark state side chain of Q513), and those in the antechamber site (see text for details). In all cases the Q513-FMN O4 hydrogen bond distance is used as a proxy for Q513 conformation.

Dark state, F434Y (3 trajectories)									
Q513-O4 distance (Å)	O4 site occupancy (# of waters)			N5 site occupancy (# of waters)			Antechamber site occupancy (# of waters)		
	0	1	2+	0	1	2+	0	1	2+
< 3.5	0.01 ± 0.00	0.03 ± 0.01	0.00	0.03 ± 0.01	0.01 ± 0.01	0.00	0.01 ± 0.00	0.02 ± 0.01	0.01 ± 0.00
3.5-6.5	0.23 ± 0.04	0.46 ± 0.04	0.06 ± 0.02	0.36 ± 0.03	0.40 ± 0.04	0.00	0.26 ± 0.03	0.34 ± 0.03	0.16 ± 0.02
> 6.5	0.11 ± 0.02	0.09 ± 0.02	0.00	0.14 ± 0.02	0.06 ± 0.02	0.00	0.14 ± 0.03	0.05 ± 0.01	0.01 ± 0.00
Light state, F434Y (3 trajectories)									
Q513-O4 distance (Å)	O4 site occupancy (# of waters)			N5 site occupancy (# of waters)			Antechamber site occupancy (# of waters)		
	0	1	2+	0	1	2+	0	1	2+
< 3.5	0.14 ± 0.03	0.00	0.00	0.14 ± 0.03	0.00	0.00	0.02 ± 0.01	0.09 ± 0.03	0.03 ± 0.01
3.5-6.5	0.41 ± 0.04	0.11 ± 0.03	0.00	0.48 ± 0.04	0.05 ± 0.02	0.00	0.41 ± 0.05	0.07 ± 0.01	0.04 ± 0.01
> 6.5	0.08 ± 0.02	0.23 ± 0.04	0.03 ± 0.01	0.32 ± 0.04	0.02 ± 0.01	0.00	0.26 ± 0.03	0.07 ± 0.01	0.01 ± 0.00

Table SI3: Observed photokinetics of other LOV domains. Decay times of the triplet state in other LOV domains are collected. As: *Avena sativa*; Cr: *Chlamydomonas reinhardtii*; Ac: *Adiantum capillus-veneris* phy3, Bs: *Bacillus subtilis*. CrLOV1 (*22*), CrLOV1-C57S (*23*), CrLOV2 (*24*), AcLOV (*25*), FMN (*25*), BsYtvA (*26, 27*), and riboflavin (*28*). *Data (*20*) obtained from AsLOV2 in Tris buffer; in this study, AsLOV2 samples were purified in sodium phosphate buffer.

	τ_{Fl}	τ_{IC}	τ_{ISC}	$\tau_{Triplet\ State}$	$\tau_{adduct\ decay}$
WT AsLOV2	2 ns	7.4 ns	3.3 ns	2.49 µs	85 s
AsLOV2-F434Y	322 ps 1.40 ns	847 ps 4.49 ns	537 ps (30 %) 2.33 ns (70 %)	0.93 µs (33 %) 3.02 µs (64 %)	7.8 s
AsLOV2-Q513N					37.3 s
WT AsLOV2*				6 µs	35 s
AsLOV2-I16L*					19 s
AsLOV2-I16V*					5 s
AsLOV2-N38S*					< 1 s
AsLOV2-K2R/I16V*				12 µs	5 s
CrLOV1-WT	2.9 ns		2.9 ns	800 ns (80 %) 4 µs (20 %)	
CrLOV1-C57S			4.6 ns	3 µs (25 %) 27 µs (75%)	
CrLOV2-WT				500 ns	
CrLOV2-C250S				12 µs (90 %) 287 µs (10 %)	
AcLOV2					
YtvA-LOV	3.3 ns	7.28 ns	1.8 ns	1.6 µs	43 min
FMN	4.7 ns	34 ns	7.8 ns	-	-
Riboflavin	5 ns	14 ns	13.5 ns	-	-

Table SI4: The rate constants in homogeneous model for primary photodynamics of AsLOV2-

Parameter		**WT (A)**	**F434Y (B)**	**F434Y (C)**
Weight	population I	100 %	100 %	37 %
	population II	-	-	63 %
Timeconstants 1	$k_{I,vib,IC}$	$(0.6\ ps)^{-1}$	$(0.6\ ps)^{-1}$	$(0.6\ ps)^{-1}$
	$k_{II,vib,IC}$	-	-	$(0.5\ ps)^{-1}$
Timeconstants 2	$k_{I,ISC}$	$(2.14\ ns)^{-1}$	$(903\ ps)^{-1}$	$(389\ ps)^{-1}$
	$k_{II,ISC}$	-	-	$(1.48\ ns)^{-1}$

WT (A), F434Y (B), and in the proposed static inhomogeneous model for F434Y (C).

Figure SI1

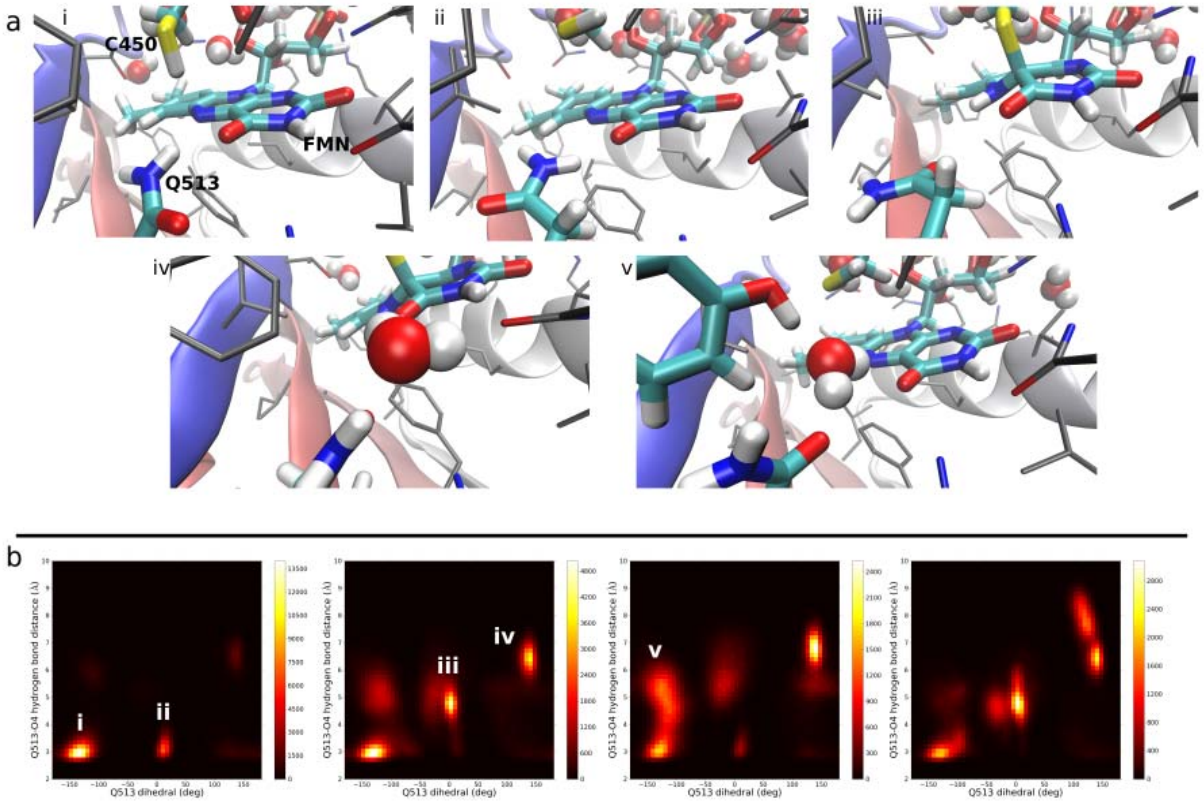

Figure SI1: Conformations of the Q513 side chain observed during wildtype (WT) and F434Y simulations. (a) Representative snapshots of five commonly observed conformations, taken from D WT (i-ii), L WT (iii-iv), or D F434Y (v) simulations. i and iii show the dark and lit states resulting from the sulfur of C450 being close to FMN (conformation I), and ii and iv correspond to dark and lit states resulting from conformation II in which there is a longer distance between C450 and FMN. (b) Histograms plotting the occupancy (in number of MD frames) of different values of the distance between the N atom of Q513 and the O4 atom of FMN, and the (imaginary) dihedral angle formed by the N, Cα, Cγ, and Cδ atoms of Q513. Conformational regions corresponding to the states from panel (a) are indicated in the plot for the simulation from which the snapshot was taken.

Figure SI2

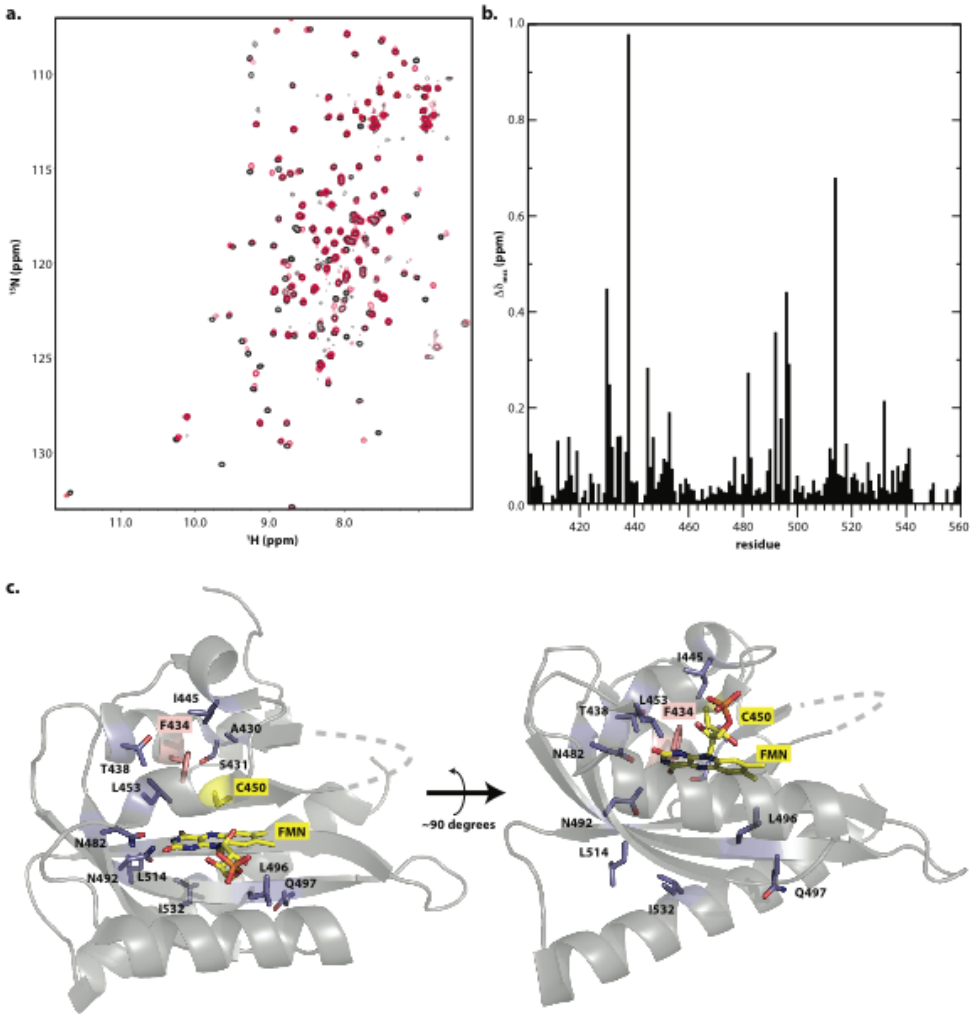

Figure SI2: Characterization of the structural changes induced by F434Y point mutation as ascertained by solution NMR spectroscopy. (a). Overlay of $^{15}N/^{1}H$ HSQC spectra of wildtype AsLOV2 (black) and F434Y (red), indicating minimal perturbation overall caused by the point mutation. (b). Minimum chemical shift difference analysis (*17*) of the spectral changes observed in panel (a), calculated as described. (c). Mapping of minimum chemical shift changes onto dark state crystal structure of AsLOV2 (PDB entry 2V0U) (*7*). Residues with backbone amides experiencing minimum chemical shift changes > 0.2 ppm are colored blue; F434 is colored pink; C450 and the FMN chromophore are colored yellow.

Figure SI3

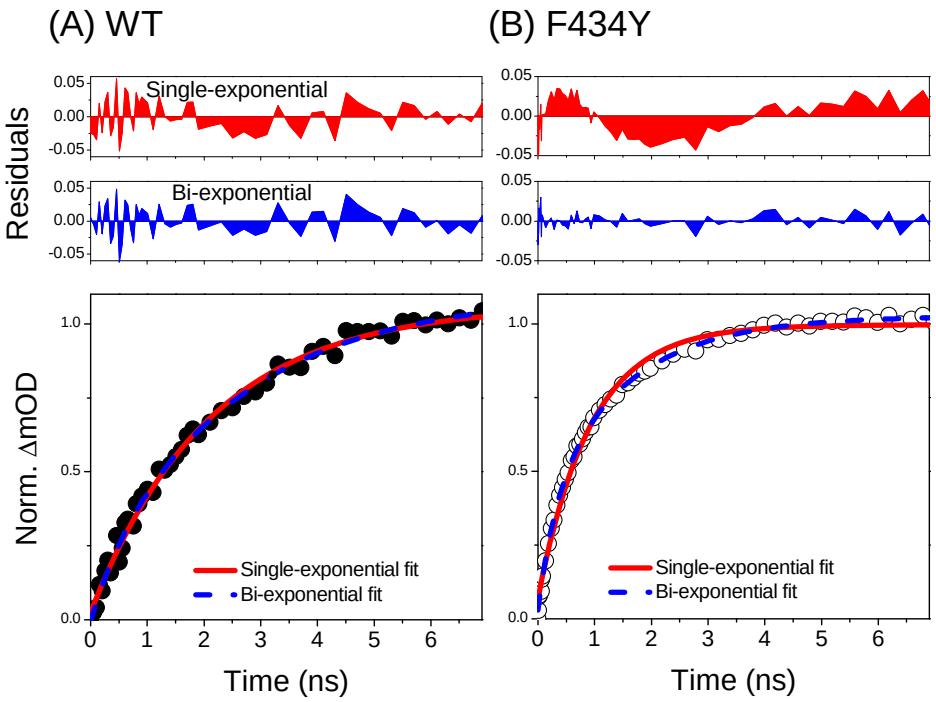

Figure SI3: 550 nm ultrafast kinetics analyzed with single- (dashed blue lines) and bi-exponential (solid red lines) decay functions (single wavelength fits). (A) The wildtype AsLOV2 kinetics are fit well with a single-exponential decay with a 2099 ns time-constant. (B) Fitting the F434Y kinetics requires two time constants of 322 ns (33%) and 1466 ns (66%) as indicated by residuals.

Figure SI4

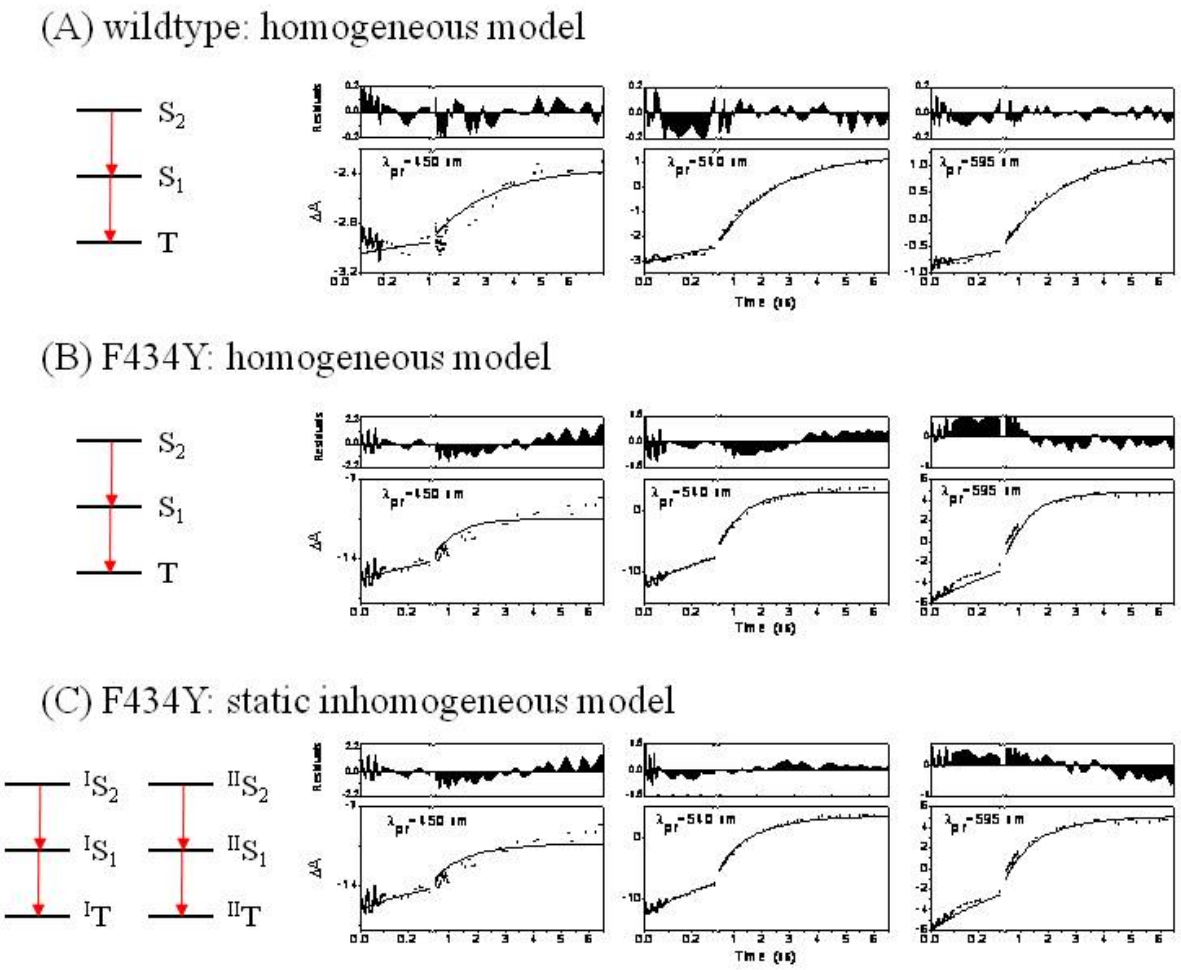

Figure SI4: Global analysis of ultrafast data to simple models (A) wildtype AsLOV2, single population homogeneous model; (B) F434Y fit with a single population homogeneous model; (C): F434Y fit with a two-population *static* inhomogeneous model. Kinetics of F434Y is explained under the assumption that population I and population II are not interchanging.

Fig. SI5

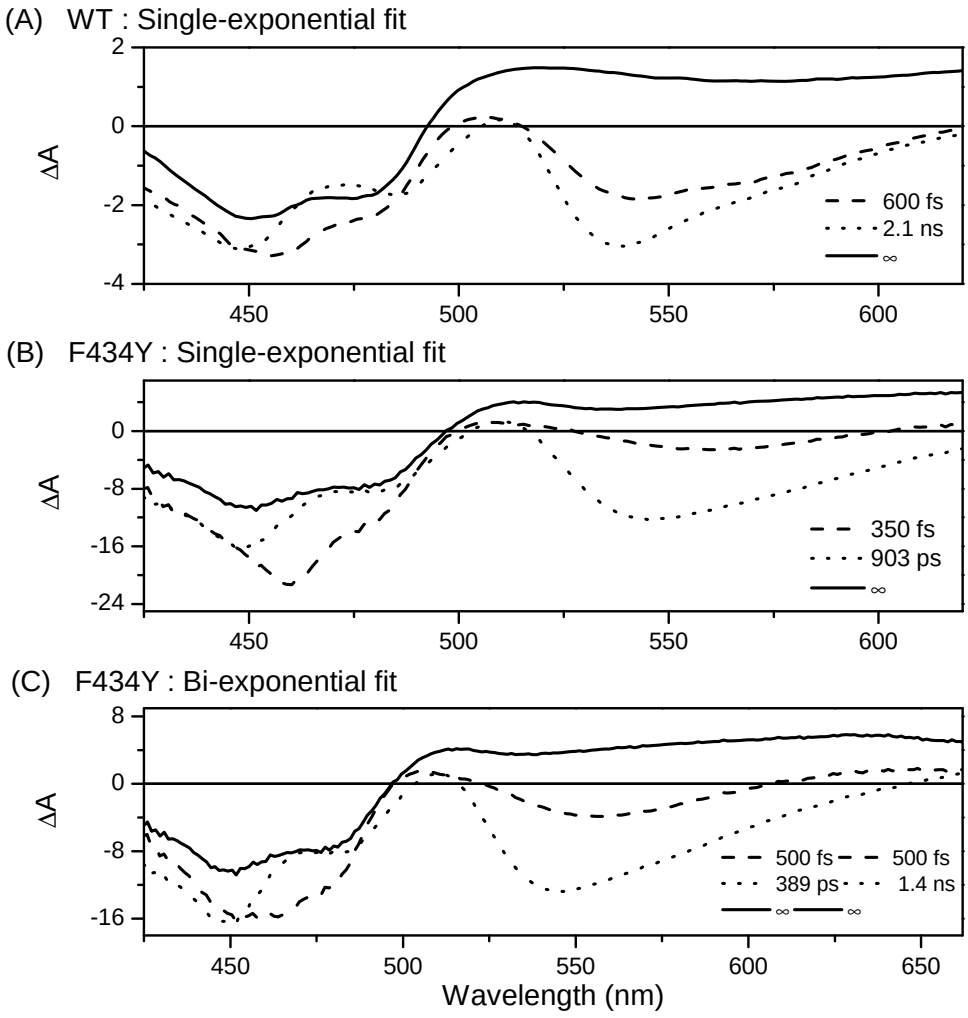

Figure SI5: The Species Associated Difference Spectra (SADS) to the three global analysis scenarios from Figure SI2. (A) wildtype AsLOV2: homogeneous model; (B) F434Y: homogenous model; (C) F434Y: *static* inhomogeneous model.

Figure SI6

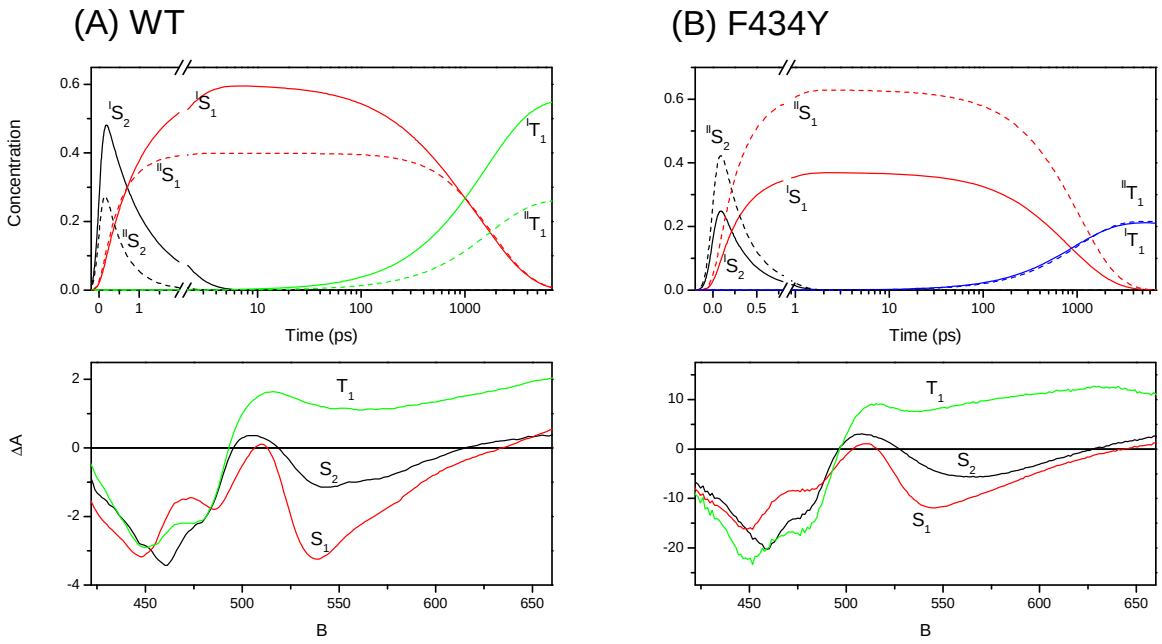

Figure SI6: Estimated concentration profiles and SADS extracted from the global analysis using the *dynamic* inhomogeneous model of Figure 7. The populations are: S_2/hot S_2 (black), S_1 (red) and triplet (green). Dashed (conformer I) and solid (conformer II) lines indicate dynamics of the sub-populations.

Figure SI7

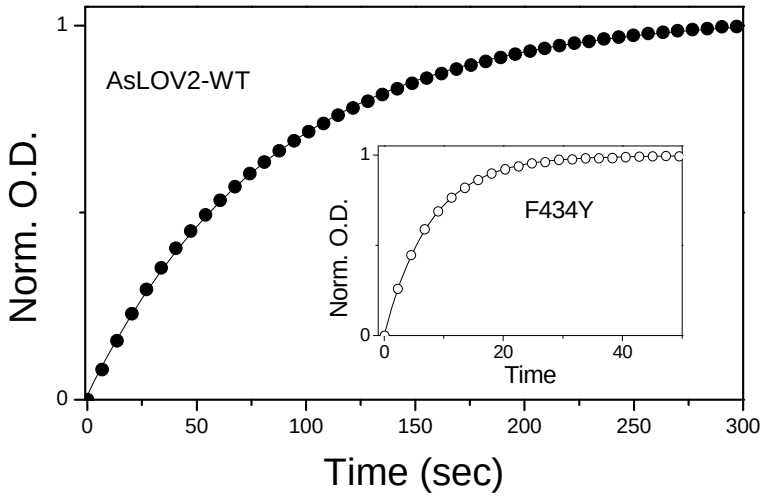

Figure SI7: Dark recovery kinetics of wildtype AsLOV2 and the F434Y mutant (inset). The collected data points were fitted using a first-order rate equation to obtain the dark state recovery time constants of 85 sec and 7.79 sec respectively.

Figure SI8

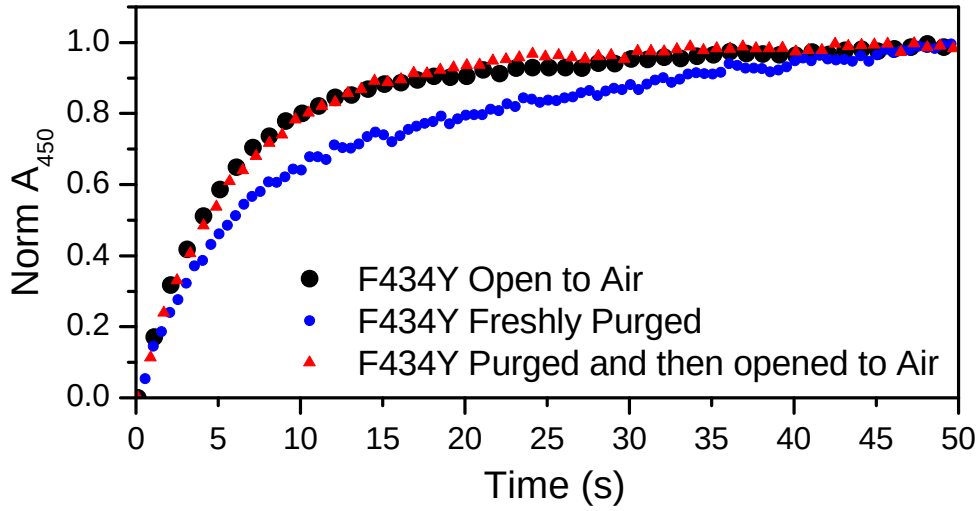

Figure SI8: Oxygen sensitivity of the dark recovery kinetics measured for the F434Y mutant. Kinetics measured during exposure to ambient air (black circles) are contrasted with the kinetics of an argon purged sample immediate after purging (blue circles) and after purged sample was exposed to air for 5 minutes (red triangles). All concentrations and illumination levels are held constant.